Facile Method for Large Scale Alignment of One Dimensional Nanoparticles and Control over Myoblast Orientation and Differentiation

Xingjie Zan,[†,§] Sheng Feng,[†,§] Elizabeth Balizan,[†] Yuan Lin,[‡,*] and Qian Wang[†,*]

[†]Department of Chemistry and Biochemistry, University of South Carolina, Columbia, South Carolina 29208, United States, and [‡]State Key Laboratory of Polymer Physics and Chemistry, Changchun Institute of Applied Chemistry, Chinese Academy of Sciences, Changchun, Jilin 130022, PR China. [§]X. Zan and S. Feng contributed equally.

ABSTRACT

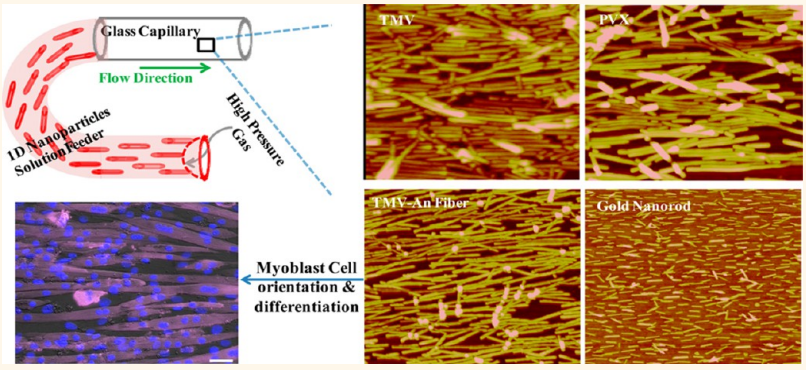

A facile and robust method to align one-dimensional (1D) nanoparticles (NPs) in large scale has been developed. Using flow assembly, representative rod-like nanoparticles, including tobacco mosaic virus (TMV), gold nanorods, and bacteriophage M13, have been aligned inside glass tubes by controlling flow rate and substrate surface properties. The properties of 1D NPs, such as stiffness and aspect ratio, play a critical role in the alignment. Furthermore, these hierarchically organized structures can be used to support cell growth and control the cell orientation and morphology. When C2C12 myoblasts were cultured on surfaces coated with aligned TMV, we found that nanoscale topographic features were critical to guide the cell orientation and myogenic differentiation. This method can therefore be used in the fabrication of complex assemblies with 1D NPs and have wide applications in tissue engineering, sensing, electronics, and optical fields.

KEYWORDS: 1D nanoparticles · self-assembly · alignment · tobacco mosaic virus · myogenic differentiation · capillary

One-dimensional (1D) nanoparticles (NPs), such as nanorods and nanotubes, have become attractive building blocks for developing materials with wide applications in tissue engineering,[1] medicine,[2] electronics,[3] and optical devices.[4] In addition to their unique anisotropic shapes and shape related properties, the orientation and alignment of 1D NPs is also crucial for final material properties.[5,6] For example, it has been shown that both electrical and thermal conductivity of carbon nanotubes increases along the alignment direction, and the enhancement was strongly dependent on the degree of alignment.[7,8] Therefore, a variety of methods have been proposed for integrating organized 1D NPs into devices. One typical method is based on the interaction between 1D NPs and supporting substrates, where the orientation of 1D NPs is directed by surface chemical functionalities,[9] micropatterns fabricated by lithography,[10] or the capillary force at a contact line during a drying process.[11] Another strategy to direct the orientation of 1D NPs is to employ an external force. The external force can be a contact shear force,[12−14] electric field,[15] fluid flow,[3,16,17] or surface pressure.[18] For example, using shear force generated by

* Address correspondence to wang263@mailbox.sc.edu, linyuan@ciac.ac.cn.

Received for review October 18, 2012 and accepted September 4, 2013.

Published online September 04, 2013
10.1021/nn403908k

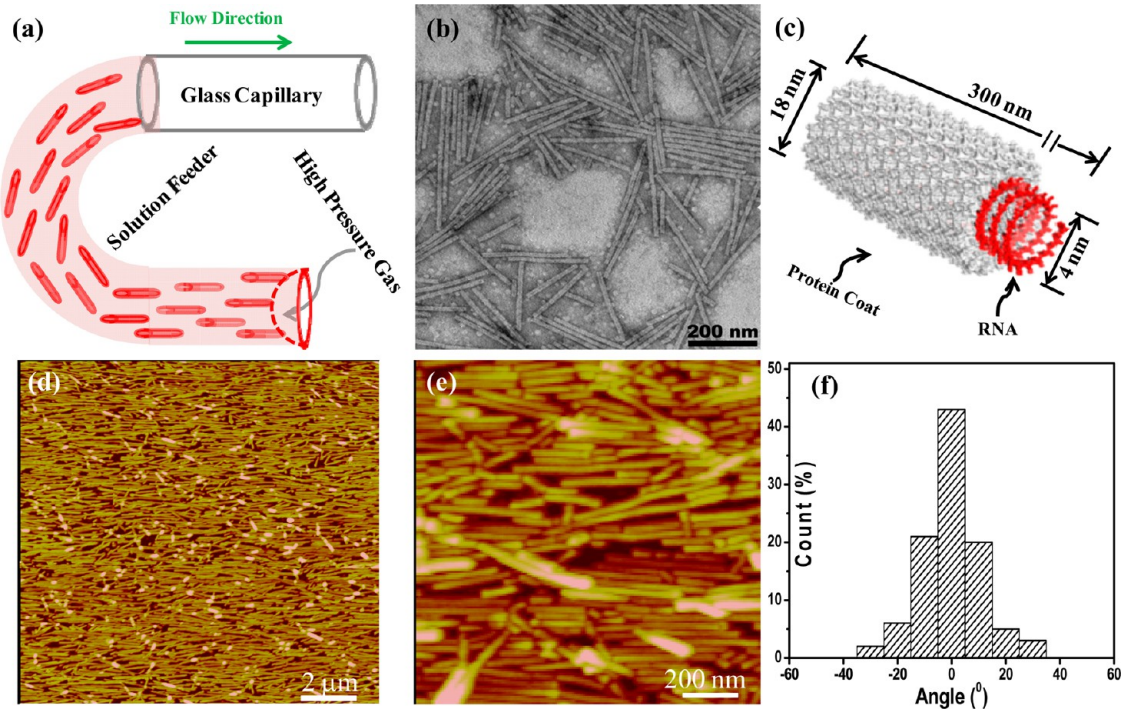

Figure 1. (a) Schematic illustration of experimental setup. One end of feeder tube is connected to the capillary, while the other end is kept open for filling of 1D NP solutions and subsequent high pressure gas. 1D NP solution is only filled into the plastic tube, keeping the glass capillary tube empty. Then the solution in the feeding tube is driven through the capillary tube by the high pressure gas. After the NP solution flows through the capillary tube, the capillary is dried by a continuing gas flow. The arrow "→" indicates flow direction. (b) Transmission election microscopy (TEM) image and (c) structure illustration of TMV. (d) AFM image of aligned TMV on the inner surface of a capillary tube after the flow assembly, prepared with a TMV concentration of 0.05 mg·mL^{-1} and a flow rate of 200 cm·s^{-1}. (e) Magnified image of (d). (f) A histogram of TMV angular spread distribution with respect to flow direction.

fluid flow, Lieber and co-workers have demonstrated that indium phosphide, gallium phosphide, and silicon nanowires were aligned by flowing nanowire suspensions through polydimethylsiloxane templated microchannels.[16] Inspired by the simple physics behind this fluid flow method, we seek to expand it beyond the original microchannel setup and develop a cost-effective, time-saving, high-throughput, and versatile method to control 1D NPs orientation in large scale.

The alignment of cells is critical for the *in vivo* function of many cells or tissues, including neural cells,[19] corneal tissue,[20] vascular tissue,[21] musculoskeletal tissue[22] and myocardial tissue.[23] Therefore, directing cell orientation and differentiation by mimicking the organization of real tissue or extracellular matrix (ECM) proteins is an emerging topic for the purpose of tissue engineering.[24,25] Taking advantage of 1D NPs to direct cell growth and differentiation has been demonstrated by Werner and coauthors, where aligned 1D collagen fiber enhanced myotube organization and length and modulated the growth and fate of mesenchymal stem cells.[26] In our previous studies, aligned bacteriophage M13 thin film was utilized to guide cells oriented along the M13 aligned direction through directing the secreted ECM protein.[27,28] In addition, the confined spaces, perpendicular to the capillary, provided by tobacco mosaic virus (TMV) patterned rings were used to direct the perpendicular orientation of smooth muscle cells to the capillary, which is believed to have great potential to develop a vascular grafting.[29]

In this study, using flow assembly, representative rod-like nanoparticles, including TMV, gold nanorods, and bacteriophage M13, have been aligned inside glass tubes by controlling flow rate and substrate surface properties (Figure 1a). TMV has the shape of a hollow cylinder (18 nm in diameter, 300 nm in length, and 4 nm cavity), consists of 2130 identical subunits that assemble helically around single strand RNA (Figure 1b,c), and can be modified chemically and genetically.[30−33] The uniformly ordered nanostructure and well-defined geometry of TMV provides a unique building block for nanomaterial development and biomedical applications.[30−40] Therefore, TMV was chosen to optimize the experimental setup and assembly conditions. When C2C12 myoblasts were cultured on surfaces coated with aligned TMV, we found that nanoscale topographic features were critical to guide the cell orientation and myogenic differentiation. This method can be used to fabricate complex structures with 1D nanoparticles and will have potential applications in tissue engineering, sensing, electronics and optical fields.

RESULTS AND DISCUSSION

Setup of Experiment. The setup of the experiment is schematically illustrated in Figure 1a, which consists of

TABLE 1. Sample Preparation Conditions and Results

						results	
samples	modification[a]	surface charge	phosphate buffer concentration (mM)	flow rate ($cm \cdot s^{-1}$)	washed before dry[b]	HPW (°)[c]	surface coverage (%)
typical	$chitosan_1$	+	0	200	N	28 (Y)	96
control 1	$chitosan_1$	+	0	0	N	176 (N)	44
control 2	$PDDA_1$	+	0	200	N	29 (Y)	88
control 3	$APTES_1$	+	0	200	N	29 (Y)	87
control 4	$(PDDA/PSS)_3$	−	0	200	N	170 (N)	5
control 5	$(PDDA/PAA)_3$	−	0	200	N	169 (N)	8
control 6	glass	neutral	0	200	N	172 (N)	10
control 7	$chitosan_1$	+	50	200	N	46 (N)	57
control 8	$chitosan_1$	+	0	200	Y	30 (Y)	63

[a] The subscript in this column noted as the modification cycle number, and the modification methods are shown in the Experimental Section. [b] The sample was washed by water (Y) or not (N) before it was dried. [c] The aligned structure as Figure 1e can be obtained (Y) or not (N).

a glass capillary tube (inner diameter ~0.16 cm, length ~15 cm), a solution feeder tube (plastic tubing with inner diameter ~0.15 cm), and high pressure gas cylinder with a valve to control gas and subsequent fluid flow rate. One end of the plastic feeder tube is connected to the glass capillary tube, and the other end is left open for filling 1D NP solution, and subsequent connection to a high pressure cylinder. All connection areas are sealed to avoid the leaking of solution or gas. In this case, the NP solution is driven through the glass capillary by the high pressure gas once the cylinder valve is open.

Before the fluid flow, the capillaries were immersed in chitosan solution (1 $mg \cdot mL^{-1}$ in 0.1% acetic acid at pH 6.5) for 20 min and then dried by the N_2 flow. In a typical experiment, 10 mL of TMV (0.05 $mg \cdot mL^{-1}$) was filled into a plastic feeder tube, driven through a capillary by a fluid flow rate of 200 $cm \cdot s^{-1}$, and then dried completely with air flow. TMV particles were distributed evenly with 96% surface coverage and an overall alignment along the long axis of the capillary, as shown under AFM (Figure 1d,e). More importantly, such alignment was observed on over 20 random positions in the inner surface of the glass tube, indicating a uniform coverage over the whole capillary tube. The orientation of TMV was further quantitatively assessed by analyzing angles of more than 200 nanorods with respect to flow direction. The angular spread distribution histogram of TMV is shown in Figure 1f. Over 84% TMV nanorods were aligned within ±10°, and the rest were distributed between ±10−30°. In addition, with this method, we also generated the aligned TMV in the polycaprolactone (PCL) tubes (Figure S1, Supporting Information), which is a widely used material for tissue engineering. The coverage of TMV is lower in PCL tubes than glass capillary tubes at the same prepared conditions, likely due to the difference of the surface chemistry between PCL tubes and glass capillary tubes, which will be further discussed in the next section.

Effects of Surface Properties on TMV Alignment. In order to understand the origin of the aligned structure and key factors on controlling the alignment, various control experiments were carried out. All samples and their corresponding preparing conditions were listed in Table 1. All samples were prepared under same TMV concentration (0.02 $mg \cdot mL^{-1}$) and flow rate (200 $cm \cdot s^{-1}$). After the samples were ready, at least 20 AFM images were taken for each sample from the random position of capillary tubes. On the basis of the AFM images, TMV angular spread distribution histograms were obtained by analyzing the angles of more than 200 particles with respect to the flow direction, and then the histograms were simulated by Gaussian equation. The alignment degrees of 1D NPs were also evaluated by the half-height peak width (HPW), *i.e.* the peak width at the half-height of peak. The smaller the HPW number is, the better alignment the sample has.[16] The surface coverage was used to estimate the coating efficacy of this method. The results are listed in Table 1. In the control 1, the experiment was performed under the described condition, but no fluid flow was applied. Only randomly distributed TMV (Figure 2a) with 44% surface coverage was observed. The value of HPW is 176°, which is very close to the totally random distribution of 180°. This result indicates that such aligned TMV nanorod structure was generated by the shearing force from the solution flow.

The interaction between TMV and the substrate plays an important role on forming this oriented structure. This interaction depends on two major factors: the surface energy and the surface charge distribution. Because the p*I* of TMV is around 3.4,[41] in our general protocol, chitosan was used to give the capillary a positively charged internal surface. The water contact angle of chitosan coated surface was 48 ± 2°. In control 2 and 3, two other cationic compounds, poly(diallyldimethylammonium chloride) (PDDA) and (3-aminopropyl)triehoxysilane (APTES), were used to obtain similar positively charged surface, but different surface energy. Simply judged from the water contact angles, control 2 has higher while control 3 has lower surface energy than chitosan modified surface (water

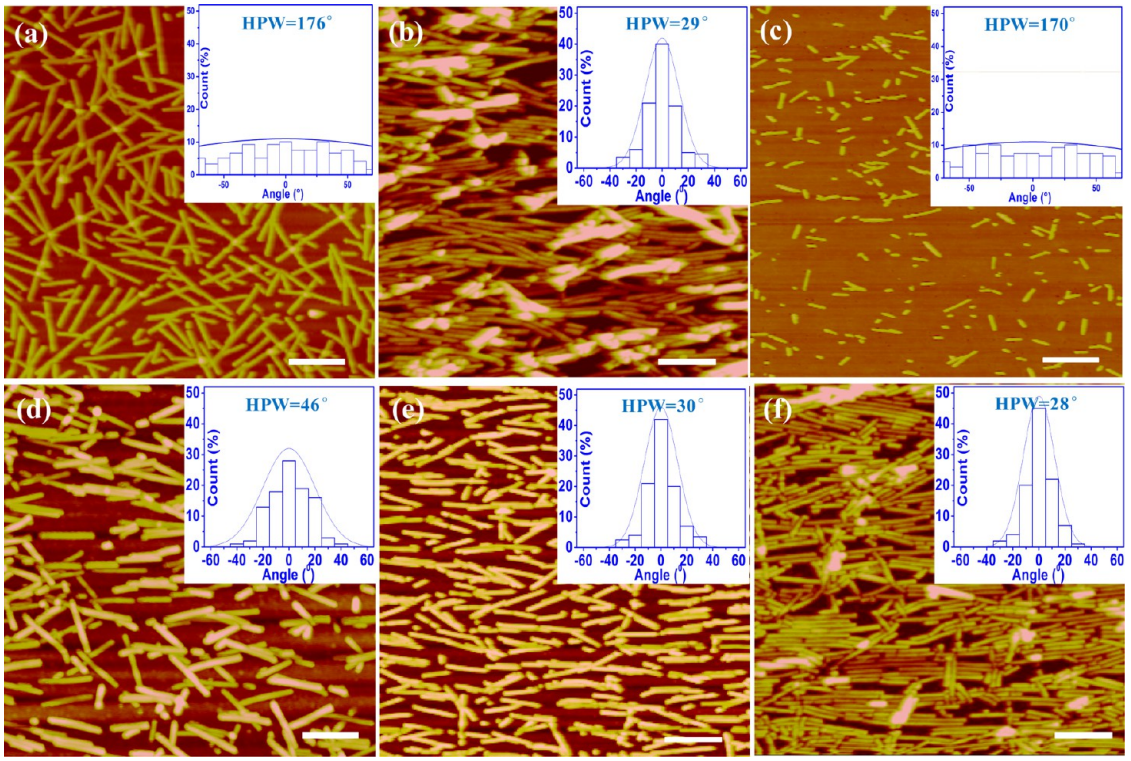

Figure 2. AFM images of (a) control 1, (b) control 2 (control 3 gave similar results), (c) controls 4−6, (d) control 7, (e) control 8, and (f) a typical sample after being immersed into PBS overnight at 37 °C. All scale bars indicate 200 nm. The insets are the histograms of TMV angular distribution at corresponding flow rates. The curve in each histogram is fitted by Gaussian equation based on the histogram data. The angle distribution histograms were obtained by statistical analysis of angular distribution of ~200 TMV particles with respect to the flow direction.

contact angles were 30 ± 1° and 81 ± 2°, respectively). After the fluid flow, similar assembly morphologies were obtained (Figure 2b) in both cases. Their comparable HPW and surface coverage percent values with the typical sample (Table 1) indicate the surface energy was not a key factor on controlling the alignment. On the other hand, if the surface was negatively charged or neutral, as shown in controls 4−6, the high HPW were generated (Table 1), suggesting TMV particles were randomly distributed (Figure 2c). In addition, the surface coverage of controls 4−6 are much lower than controls 2 and 3 and typical chitosan modified samples (Table 1) because of electrostatic repulsion between TMV and the substrate. These results revealed that the electrostatic interaction between TMV and the substrate is critical for the formation of the aligned structure. To confirm this hypothesis, we increased the ionic strength of the TMV solution by adding 50 mM phosphate buffer (pH 7.0) to weaken the electrostatic attraction between TMV and chitosan coated surface (control 7). As expected, weakening attraction resulted in increased HPW and decreased surface coverage (Table 1 and Figure 2d), indicating much less TMV particles deposited and a worse alignment. Overall, the shearing force generated by fluid flow can drag TMV particles to align along the flow direction, *i.e.*, the long axis of capillary tube, because of its anisotropic shape. Furthermore, the attractive force between TMV and capillary internal surface plays an important role in pinning the TMV particles on the surface.

Finally, we found that, once it was dried by following gas immediately, the deposited TMV with aligned structure gave almost no change on the HPW and slight decrease in surface coverage after it was immersed into PBS solution at 37 °C for 24 h (Figure 2f). This feature suggests that it is a relatively stable environment for the cell study. However, TMV particles could be washed off if the sample was not dried completely by the gas flow (Figure 2e), which gave a decreased surface coverage and a similar HPW (control 8 in Table 1).

Effect of Flow Rate on TMV Alignment. For testing the effect of flow shearing force on the alignment of TMV, different flow rates ranging from 50 to 200 $cm \cdot s^{-1}$ were applied to prepare samples with fixed TMV concentration at 0.02 $mg \cdot mL^{-1}$. On the basis of the AFM images (Figure 3a−d), TMV angular spread distribution histograms were obtained by analyzing the angles of more than 200 particles with respect to the flow direction, and then the histograms were simulated by Gaussian equation (insets of Figure 3a−d). Obviously, with the increased flow rate, the width of TMV angular distribution was narrowed, while the distribution near angle 0° in the histograms increased. To evaluate the alignment degree of 1D NPs, the HPW was plotted against flow rate and shown in Figure 3e. The HPW decreased from 52° to 28° with the increased flow rate

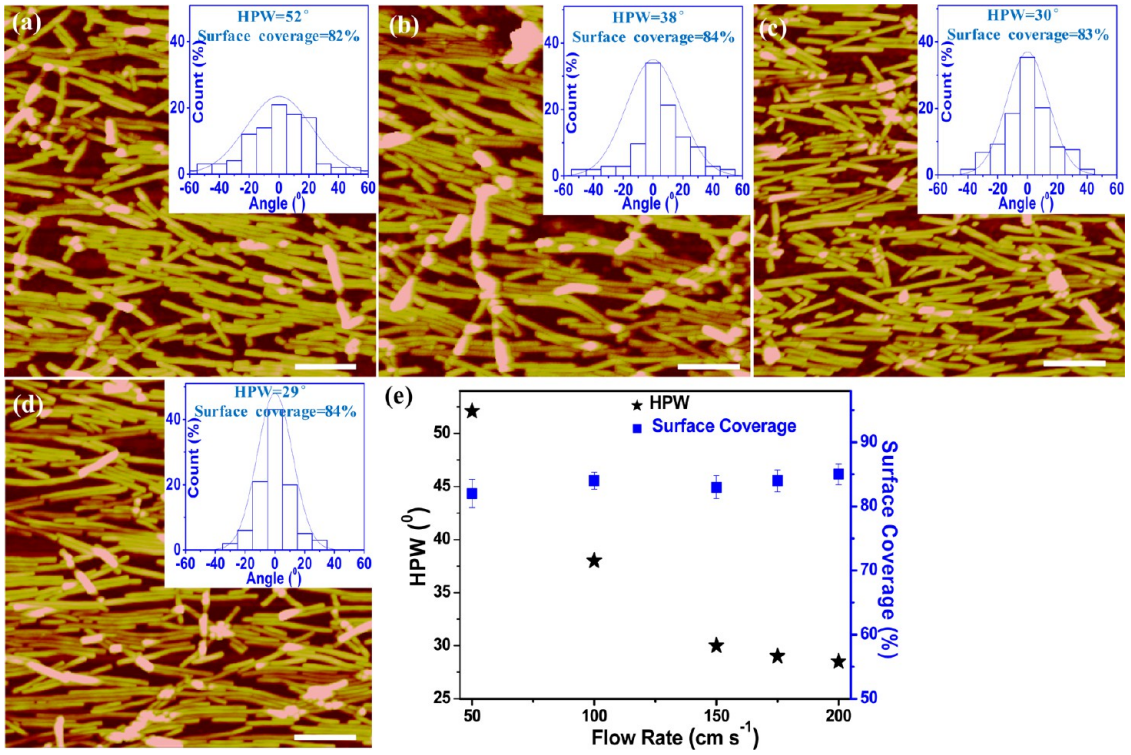

Figure 3. AFM images of flow assembly TMV on chitosan modified capillary tube at different flow rates: (a) 50, (b) 100, (c) 150, and (d) 175 cm·s^{-1}. The TMV concentrations were 0.02 mg·mL^{-1}. The insets are the histograms of TMV angular distribution at corresponding flow rates. The curve in each histogram was fitted by Gaussian equation based on the histogram data. The angle distribution histograms were obtained by statistical analysis of angular distribution of ~200 TMV particles with respect to the flow direction. (e) The dependence of HPW direction on flow rate. All scale bars indicate 200 nm.

from 50 to 200 cm·s^{-1}. It implies that the alignment of TMV was improved greatly by increasing the flow rate, which is consistent with the previous report.[16] This phenomenon can be explained from the Newton shear flow theory: the shearing force increases proportionally with the flow rate. Because the TMV particles are aligned in response to the shearing force, a higher flow rate means a bigger shearing force and hence leads to a better alignment. The best alignment in the experimental flow range for this system is that about 84% TMV nanorods were aligned within ±10° at flow rate 200 cm·s^{-1}. Thus the flow rate of 200 cm·s^{-1} was used for next sample preparation if it is not mentioned specifically. In all tested flow rate ranges, samples exhibited constant surface coverage around 85%, as shown in Figure 3e.

Influence of TMV Concentration on Alignment and Substrate Coverage. The surface coverage of the TMV can be controlled by the TMV concentration. As shown in Figure 4a–c, the average coverages are about 95, 86, and 50% for the TMV concentration at 0.05, 0.02, and 0.005 mg·mL^{-1}, respectively. In addition, the decreased concentration also led to the slightly decreased alignment, as revealed by the HPW of the simulated peaks (insets of Figure 4a–c). These results are consistent with previous report.[42] In addition, the differences in coverage in microscale as well as the alignment are important for controlling cell orientation and differentiation, which will be further discussed in the following cell study section.

Influence of the 1D NP Physical Properties on the Alignment. We extended our method to other 1D NPs and showed how the physical properties affect the fluid flow assembly. A selection of different kinds of representative 1D NPs were studied, including potato virus X (PVX),[43] TMV-Aniline hybridized fibers,[41,44] filamentous bacteriophage M13,[45] and gold nanorods (GNRs).[5] The selection of these 1D NPs is due to not only their representatives in their respective family, but also their distinctive physical properties (aspect ratio and rigidity). The preparation and purification of the selected 1D NPs are described in detail in the Experimental Section. The physical properties of these 1D NPs are listed in Table 2, and TEM images are shown in Figure 5a–d.

We fixed the flow rate at 200 cm·s^{-1} and the 1D NPs concentration at 0.02 mg·mL^{-1} during the flow assembly process, and the final results were observed by AFM (Figure 5e–h). The particle alignment with respect to the fluid flow direction was analyzed, and corresponding angular spread distribution histograms were obtained and shown in the insets of the Figure 5e–h. The alignment degree was evaluated by the HPW, as plotted in Figure 5e. To study how the rigidity and aspect ratio affect the alignment, we set those 1D NPs into several pairs for comparison, based on comparable rigidity or aspect ratio.

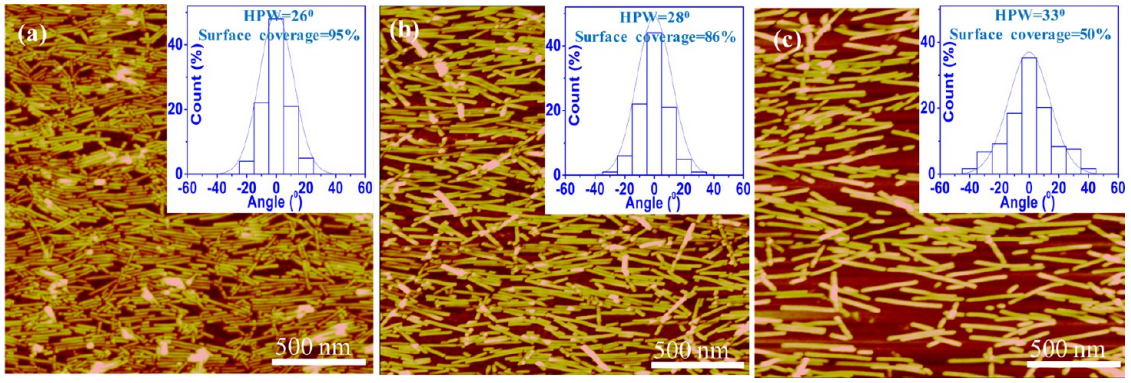

Figure 4. AFM images of flow assembly with (a) 0.05, (b) 0.02, and (c) 0.005 mg·mL^{-1} of TMV on chitosan modified capillary tubes at a fixed flow rate of 200 cm·s^{-1}. The insets are their corresponding angular spread distribution histograms of TMV with respect to the flow direction and HPW values.

TABLE 2. Parameters (Aspect Ratio and Modulus) Of Different 1D NPs Used in Experiments

			TMV-Aniline		
1D NPs	TMV	PVX	fiber	M13	GNRs
contour length *L* (nm)	300	550	4000	880	350
diameter (nm)	18	13.5	18.5	4.5	25
aspect ratio	17	41	216	196	16
persistent length *P* (μm)	~1000[46]	—	—	1.27[47]	—
modulus (GPa)	1.1[48,49]	0.85[48]	1.23[49]	0.62[48,49]	64[50]

The role of rigidity on the alignment can be illustrated by comparing alignment degrees of two 1D NPs with similar aspect ratio, but different modulus, *i.e.*, GNRs and TMV. The HPW of GNRs (14°) is much narrower angular spread than TMV (28°) because of the 45-fold higher modulus of GNRs (Figure 5h *versus* Figure 1d), suggesting that a higher rigidity of 1D NPs results in a better alignment. The dependence of alignment on the aspect ratio of 1D NPs could be reflected when comparing two 1D NPs with similar modulus, but different aspect ratio, *i.e.*, TMV and TMV-Aniline fiber. The HPW of TMV-Aniline fiber had been narrowed to 16° from 28° with the increased length from 300 nm to 4 μm (Figure 5f *versus* Figure 1d). Similarly, PVX, a little bit longer than TMV but with comparable rigidity, showed a better alignment (25° in HPW) than TMV (28° in HPW) (Figure 5e *versus* Figure 1d). Furthermore, under comparable modulus, TMV, PVX, and TMV-Aniline fiber having gradually increased aspect ratio displayed a gradual decrease in HPW. All of these results indicate higher aspect ratio of 1D NPs leads to a higher alignment degree. Comparing the HPW of TMV-Aniline fiber (16°) to M13 (44°), a much bigger difference between TMV-Aniline fiber and M13 than other pairs of 1D bio-NPs was observed because of the synergetic enhancement from longer length and higher modulus of TMV-Aniline fiber than M13 (Figure 5f *versus* Figure 5g). The surface coverage is over 90% for all tested samples except the GNRs with a 34% surface coverage (Figure 5). The low coverage of the GNRs might be caused by its surface chemistry defects.[51]

Among these 1D NPs, TMV-Aniline fiber and GNRs have higher rigidities (Table 2), thus resulting in the best alignment; *i.e.*, 95% of particles aligned within ±10° and 98% aligned within ±10°, respectively, which may have potentials in the electronic and optic applications.[52,53] Clearly, the rigidity and aspect ratio of the 1D NPs are two major factors on the alignment of the 1D NPs, which should be considered when this method is applied. The same method might be used to control the alignment of other 1D NPs if optimized fluid flow and suitable attraction between 1D NPs and substrate were applied.

Alignment and Differentiation of Myotubes. Enhancing the differentiation and alignment of cells in biomaterials is crucial for engineering functional tissues with anisotropic properties.[54] For example, in native musculoskeletal tissue, the myoblasts form aligned fibers in a highly organized manner through the fusion into the multinucleated myotubes.[22] The similar organization with the alignment also exists in myocardial tissue.[23] On the other hand, skeletal myogenesis, as a terminal differentiation process, is involved in the differentiation and fusion of proliferating mononucleated myoblasts into multinucleated myoblasts. C2C12 myoblasts have been used as a model system to study various types of muscular dystrophies *in vitro*.[55−57] Many studies have described the C2C12 patterning on different modified surfaces. For instance, microcontact printing has been used to generate fibronectin islands with different geometric cues to study the C2C12 alignment and maximize the C2C12 differentiation.[58]

Previous study revealed a 2D substrate coated with TMV or TMV mutants promotes rat bone marrow stromal cells osteogenic differentiation.[59] Using the aligned topographical features created by flow assembly described in this paper, we studied the orientation and differentiation of C2C12 myoblasts guided by the contact cues. Four kinds of aligned TMV and TMV-RGD-coated capillaries, TMVH, TMVL, RGDH, and RGDL, were prepared for cell studies. The letter H notes high coverage (starting with 0.02 mg·mL^{-1} of TMV or TMV-RGD), while L notes low coverage (starting

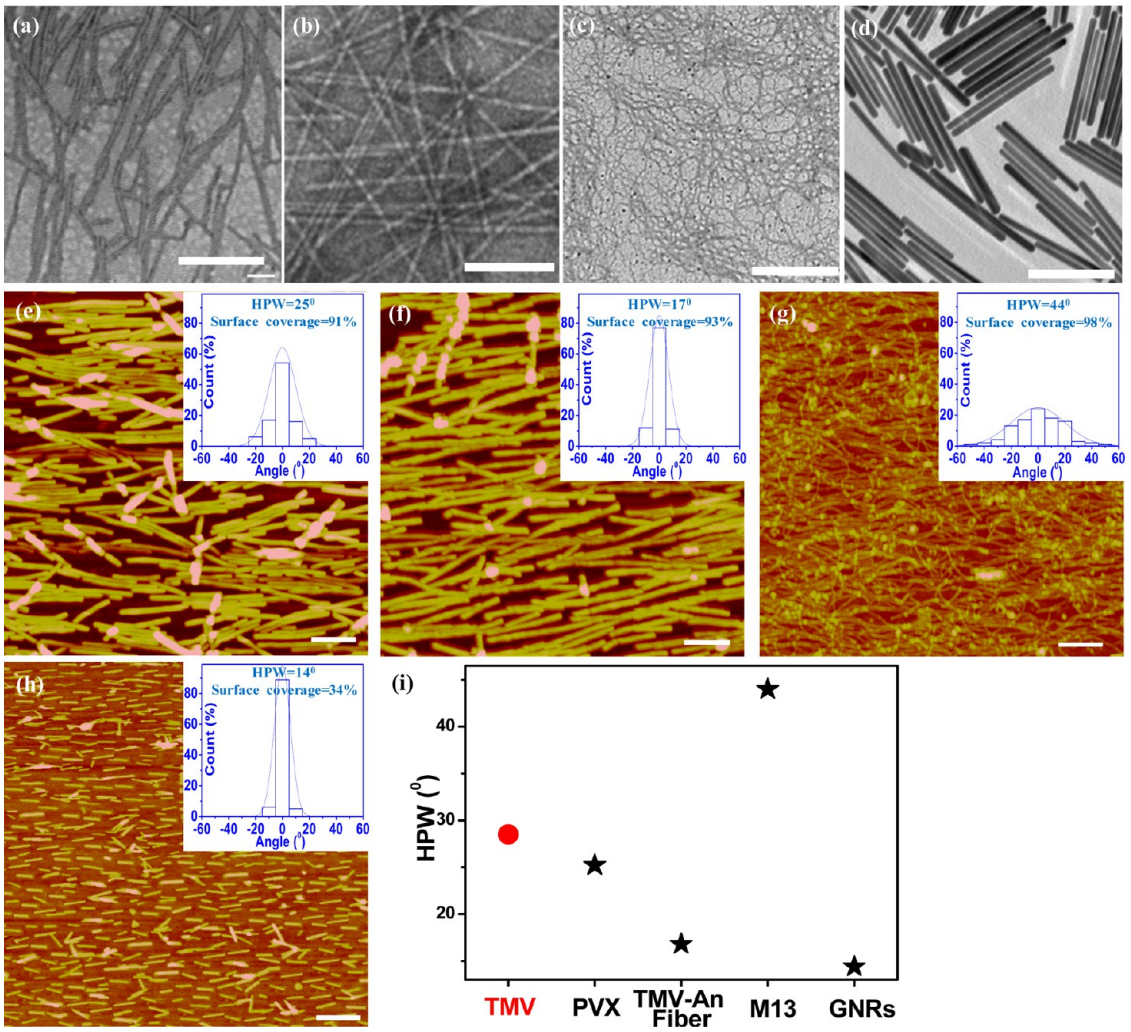

Figure 5. (a–d) TEM images of (a) PVX, (b) TMV-Aniline fiber, (c) M13, and (d) gold nanorods (GNRs). (e–h) AFM images of inner wall of capillary after flow assembly with (e) PVX, (f) TMV-Aniline fiber, (g) M13, and (h) GNRs, with fixed flow rate of 200 cm·s^{-1} and the concentration of 0.02 mg·mL^{-1} of NPs. The capillary was modified by $(PDDA/PAA)_3$ for (h), others are modified by chitosan. The insets in (e–h) are their corresponding angular spread distribution histograms with respect to the flow direction. Each histogram was obtained by statistical analysis of angular distribution of about 200 nanorods. (i) The HPW plot of different 1D NPs. The scale bars indicate 400 nm for all TEM images (a–d), 200 nm for (e), 500 nm for (f) and (g), and 1 μm for (h).

with 0.005 mg·mL^{-1} of TMV or TMV-RGD) of TMV or TMV-RGD assembled on chitosan modified capillary tubes at a fixed flow rate of 200 cm·s^{-1}, and random arranged TMV coated capillary tubes were used as the control. TMV-RGD here is the mutant TMV with inserted sequence GRGDSPG and had been proved to enhance cell attachment and stimulate osteogenic differentiation.[30,60]

We first seeded C2C12 myoblasts in capillary tubes with different TMV alignments and allowed cells to attach overnight. We did not observe any significant difference in the cells attachment to substrates among different groups. After 3 day proliferation, cells were subjected to differentiation medium (DM). Figure 6a shows the fluorescence images of the cells with myosin heavy chain (MHC) (red) and DAPI (blue) staining on different substrates after 7 days cultured in DM (representative images with low magnification are shown in Figure S2, Supporting Information). The appearance of MHC staining indicated the formation of the myotubes in all groups.

In order to quantify the degree of the myotube alignment, using ImageJ software, we measured the angles of myotubes with respect to the flow direction in 15 low magnification fluorescence images in each group and plotted the angular distribution histograms (Figure 6a). The TMVH showed the best alignment with HPW 34°, and the RGDH and RGDL showed the moderate alignment; RGDH (HPW 46°) was a little higher than RGDL (HPW 48°), and the TMVL displayed seldom alignment (HPW 126°), while there was no alignment (HPW 180°) in the random TMV coated sample. Within the deviation of ±20°, about 93% of myotubes were aligned for TMVH, and this number decreased to 81, 75, and 49% for RGDH, RGDL, and TMVL, respectively. The low degree of the alignment in TMVL might be due to low density of TMV being insufficient to guide the C2C12 cells. However, the RGDL provides the strong binding motifs, RGD peptides, for C2C12 cells, which make the low density of TMV-RGD was still

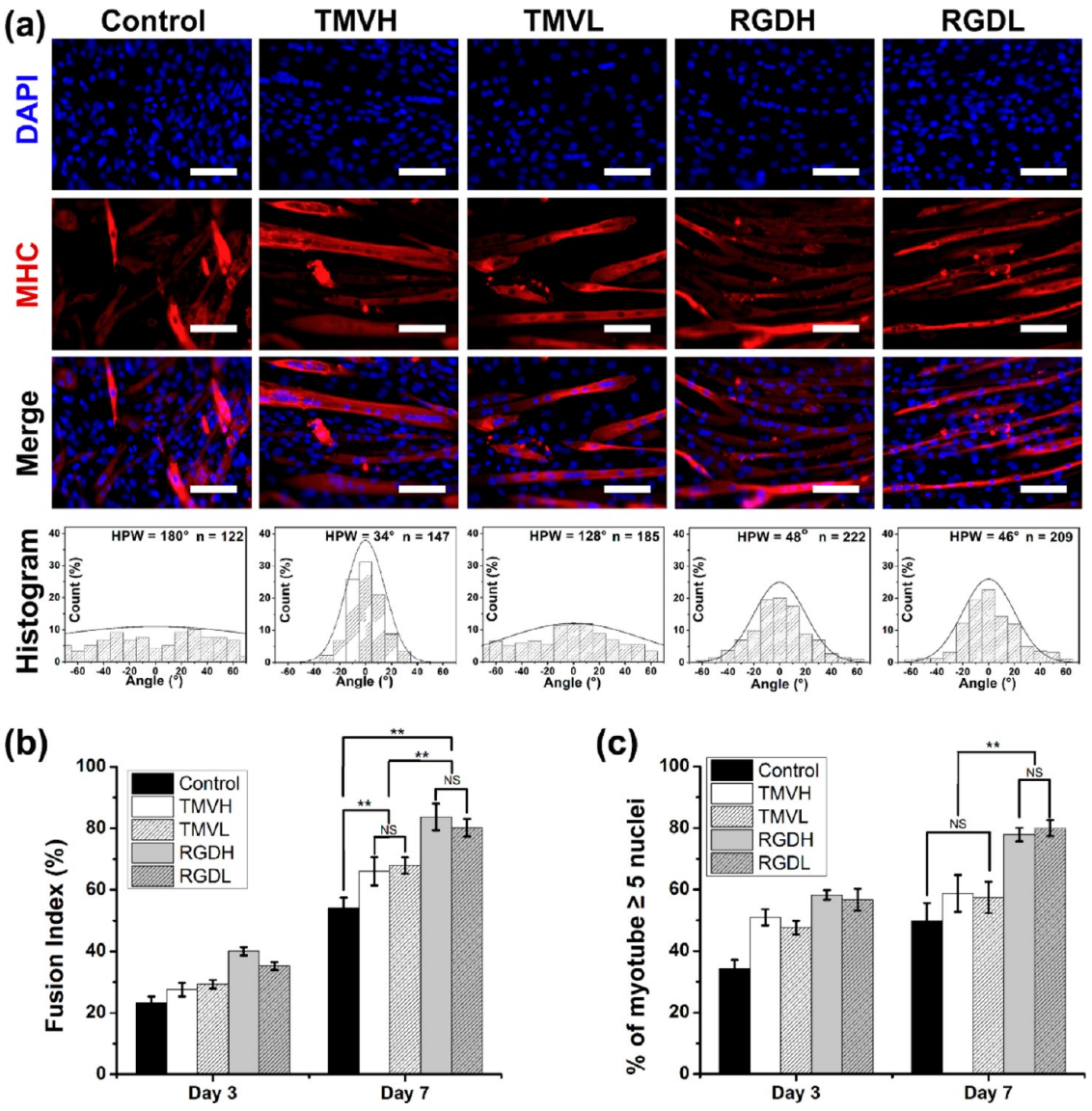

Figure 6. Alignment and differentiation of myotubes. (a) Fluorescent images of the C2C12 cells with the induction of differentiation for 7 days on the tubes with different NPs. Cells were stained for anti-MHC (red) and DAPI (blue). All scale bars indicate 100 μm. The bottom rows are corresponding histograms of the angular distribution of myotubes. (b,c) Quantification of the fusion index (b) and maturation index (c) for C2C12 cells in the tubes with different NPs. They were calculated as the ratio of nuclei number in myocytes with 2 or more nuclei over the total nuclei number and the percentage of myocyte with 5 or more nuclei, respectively. Significance: ** $p < 0.01$ and NS = not significant.

able to generate moderate guidance for the alignment of cells.

To quantify the differentiation of myoblasts, we calculated the fusion index and maturation index from the immunofluorescence images by determining the number of nuclei from multinucleated myocytes over the number of total nuclei in that field and the percentage of myotubes with 5 or more nuclei, respectively.[61] Two independent experiments were performed, and 6 random images were used to determine the fusion index and maturation index for each group. The results show that the fusion indices for cells in TMVH and TMVL groups (66.1 $\pm$ 4.6% and 67.9 $\pm$ 2.6%, respectively) significantly increased compared to the control group (54.1 $\pm$ 3.4%) ($p < 0.01$). There is no significant difference between TMVH and TMVL groups. In addition, the fusion indices for cells in RGDH and RGDL (83.7 $\pm$ 4.4% and 80.2 $\pm$ 2.9%, respectively) are significantly higher than counterparts in TMVH, TMVL, and control groups ($p < 0.01$). There is no significant difference between RGDH and RGDL groups. Furthermore, the maturation indices of cells in RGDH and RGDL groups (77.9 $\pm$ 2.6% and 80.0 $\pm$ 2.2%, respectively) are statistically higher than TMVH, TMVL, and control groups (58.8 $\pm$ 5.3%, 58.8 $\pm$ 5.3% and 49.8 $\pm$ 5.9%, respectively). Taken together, the myotubes in RGDH and RGDL had the highest level of differentiation, which is consistent with previous report that RGD peptide promotes the myotubes differentiation.[62−64] Cells in TMVH and TMVL also increased the level of differentiation compared to control groups.

Previous study has observed that the alignment of myoblasts promote their differentiation.[65] The differentiation of myoblasts depends on two critical events: the growth arrest[66] and the end-to-end contacts between myoblasts.[67] In day 3, we observed the C2C12 cells aligned along the orientation of TMV particles by F-actin staining (Figure S3, Supporting Information). The alignment of myoblasts on capillary tubes with TMV particles may enhance aligned end-to-end contacts between the cells. Therefore higher percentages of cells in groups with aligned orientation were fused to differentiate into myotubes than control group.

CONCLUSIONS

In this work, we have demonstrated that the fluid flow assembly can serve as a facile and robust method to align 1D NPs in large scale. The formation of thus aligned 1D NPs was dominated by the shearing force generated by the fluid flow, interactions between 1D NPs and substrate, and the following drying process. In addition, the alignment degree and coverage of the 1D NPs can be readily controlled by the flow rate, the concentration and the nature properties (length and modulus) of 1D NPs. In general, a better aligned structure can be produced when longer and stiffer 1D NPs are used at higher flow rate and higher concentration. This method has been used to align various kinds of 1D NPs, including rod-like viral particles, hybridized conductive nanowires, and inorganic 1D NPs. Capitalizing on the simplicity, flexibility and scalability of this method, this technique can be applied to engineer aligned 1D NPs, with wide potential applications on tissue engineering, electronic, and optical fields.

EXPERIMENTAL SECTION

Materials. Poly(acrylic acid) (PAA) (M ~450 000), poly(diallyldimethylammonium chloride) (PDDA) (20 wt % in water, M ~200 000–350 000 g/mol), poly(styrene sulfonate) (PSS) (M ~ 70 000), chitosan (high purity, M ~ 60 000–120 000), and aminopropyltriethoxysilane (APTES) were purchased from Sigma-Aldrich; the materials were used as received. Deionized water (18.2 MΩ.cm) used for rinsing and preparing all the solutions was obtained from a Millipore Simplicity 185 purification unit.

Purification of 1D NPs. The TMV, TMVRGD1 and PVX were harvested from the infected leaves according to the reported methods.[30,32,43] Briefly, 10 mM potassium phosphate buffer (pH 7.4) with 0.2% β-mercaptoethanol was added into crashed leaves, and centrifuged at 9000 rpm for 15 min. The supernatant was clarified with equal volume of $CHCl_3$ and n-butanol (1:1 ratio). Toward the aqueous supernatant, 10% PEG800 and 0.2 M NaCl were added to precipitate viral particles. After the centrifugation, the pellets were resuspended in 10 mM phosphate buffer. Finally, the pure viruses were obtained after the process of ultracentrifugation for 2.5 h at 42 000 rpm (rotor Ti 75).

Filamentous Bacteriophage M13. M13 was harvested from the infected *Escherichia coli* according to previously reported method.[44,68] Briefly, 1 L of *E. coli* ER2738 culture was grown in LB-tet media to midlog phase and infected with 1 mL of wild type M13 bacteriophage (1012 PFU/mL). The culture was incubated at 37 °C with shaking for 5–6 h and centrifuged to remove bacterial cells; the virus was collected by PEG-NaCl (20% PEG and 2.5 mol·L^{-1} NaCl) precipitation and reconstituted in Tris buffer.

Synthesis of TMV-Aniline Fibers. TMV-Aniline fibers were synthesized according to reported method.[41,69] Briefly, distilled aniline (10 L) and ammonium persulfate (10 mg·mL^{-1}, 1 mL) were added to TMV solution (1 mg·mL^{-1}, 4 mL). The reaction was taken at room temperature for 24 h. The reaction mixture was purified by dialysis for 5 h.

Synthesis of Gold Nanorods (GNRs). GNRs was synthesized according to the seed-mediate growth method.[5] The seed solution is prepared as follows: the 0.6 mL of ice-cold $NaBH_4$ (10 mM) was added into the mixture of CTAB solution (5 mL, 0.2 M) and $HAuCl_4$ (5 mL, 0.5 mM), followed by vigorous stirring of the seed solution for 3 min. The growth solution was prepared by mixing CTAB solution (0.2 M) and $HAuCl_4$ (0.5 mM) with same volume. The GNRs growth was achieved by three steps: (1) 0.2 mL of seeding solution was added into 2 mL of growth solution, which was transferred to 20 mL of growth solution after 10 s; (2) after 30 s, the solution in step 2 was poured into 200 mL growth solution; and (3) the GNRs were synthesized by incubating the solution at 25 °C for 18 h. The GNRs were purified by centrifuge with spin speed 4000 rpm for 8 min. After being redispersed into water, the GNRs were used for the assembly.

Modifications of Capillary Tube. The polyelectrolyte coated capillaries were obtained by alternatively immersing capillaries in PDDA (1 mg·mL^{-1}) for 20 min and PSS or PAA solution (1.0 mg·mL^{-1}) for 20 min, until $(PDDA/PAA)_3$ or $(PDDA/PSS)_3$ are obtained, where the number 3 indicates the number of bilayers. Water was used to rinse in between each deposition step until the desired number of layers was obtained.

For chitosan modified capillaries: By immersing into chitosan (1 mg·mL^{-1} in 0.1% acetic acid at pH 6.5), the chitosan coated capillaries were obtained. Water was used to wash before using.

The APTES modified capillaries: Capillaries were immersed into 1% APTES in ethanol/water (95:5 by volume) for 10 min, washed with pure ethanol three times, dried with nitrogen, and then incubated in a vacuum at 120–130 °C for one hour.

Flow Assembly of 1D NPs. Typically, a 10 mL solution containing 1D NPs was injected into the 1D NPs feeder (Figure 1a), whose one end was connected to nitrogen tank and the other end was connected to capillary tube. The solution was driven through the capillary tube and dried by the following gas. The flow rate of solution was controlled by the gas pressure applied to the flow.

Characterization of 1D NPs. A solution of 1D bionanoparticles was dropped on the glow-discharged Formvar-carbon coated copper grid. After drying, the sample was negatively stained with 2% uranyl acetate for TEM (Philips CM-12 transmission electron microscope at 80 keV) observation. The surface morphology was observed by AFM (SPA300, Seiko) in the tapping mode. The angles of 1D NPs were measured with ImageJ software and then plotted in angular distribution histograms. For M13, segments longer than 500 nm were measured for plot.

Cell Culture. The murine-derived muscle cell line, C2C12, was purchased from American Type Culture Collection (ATCC, Manassas, VA). Cells were cultured in Dulbecco's modified Eagle's medium (DMEM, #D6046, Sigma–Aldrich) supplemented with 10% heat inactivated fetal bovine serum (Hyclone, ThermoScientific), 100 U·mL^{-1} of penicillin and 100 μg·mL^{-1} of streptomycin (Gibco BRL, Invitrogen Corp., Carlsbad, CA, USA). C2C12 at 80–90% confluency were detached and resuspend into culture medium in a concentration of 2 × 10^6 cells per mL. The capillary tubes with TMV particles sucked the cell suspension. After 5 h, we put the tubes with cells into the 12 well plates with culture medium. After three days, the cells were shifted to differentiation medium (DM), which is DMEM supplemented with 2% horse serum (Lonza Inc.,

Williamsport, PA). The medium was replaced every other day. The time points in the figures indicate time after shifting to DM.

Immunofluorescence Microscopy. Differentiated C2C12 cells were washed once with PBS and fixed with 4% paraformaldehyde (Sigma-Aldrich, P6148) in PBS for 15 min. Cells were then blocked with 5% goat serum and 0.3% TritonX100 for 60 min in PBS. The cells were incubated with MF20 (antimyosin heavy chain (MHC), Developmental Studies Hybridoma Bank (DSHB), University of Iowa, IA) overnight at 4 °C and followed by Chromeo 642 Goat anti-Mouse IgG (Active motif, Germany) and DAPI (Sigma, USA) in dark. Cells then were imaged using an Olympus IX81 microscope. The images were analyzed with ImageJ software. The images obtained from the MHC and DAPI signals were pseudocolored red and blue respectively.

Calculation of Fusion Index and Maturation Index. The fusion index was calculated by determining the ratio of nuclei number in myocytes with two or more nuclei over the total number of nuclei. The maturation index was the percentage of myotubes with five or more nuclei. Because the cells are in the capillary tubes, cells on the edge were out of focus in images with low magnification. Cells on the edge, which were out of focus, were not used for analysis.

Statistical Analysis. Statistical analysis for mean comparison was performed by using one-way analysis of variance (ANOVA) Tukey's test in OriginPro 8.5. All data values in this study were reported as mean ± standard error of the mean.

Conflict of Interest: The authors declare no competing financial interest.

Acknowledgment. The authors are thankful to the suggestion of Dr. Xiaojun Yu and his group members of Stevens Institute of Technology for cell studies. This work was partly supported by the US NSF (CHE-0748690), the Camille Dreyfus Teacher Scholar Award, and the W. M. Keck Foundation. Y.L. and Q.W. are grateful to the financial support of the National Natural Science Foundation of China (21128002 and 21104080) and the State Key Laboratory of Polymer Physics and Chemistry of CIAC.

Supporting Information Available: Figures S1−S3. This material is available free of charge *via* the Internet at http://pubs.acs.org.

REFERENCES AND NOTES

1. Tay, C. Y.; Irvine, S. A.; Boey, F. Y. C.; Tan, L. P.; Venkatraman, S. Micro-/Nano-Engineered Cellular Responses for Soft Tissue Engineering and Biomedical Applications. *Small* **2011**, *7*, 1361–1378.
2. Chung, W. J.; Oh, J. W.; Kwak, K.; Lee, B. Y.; Meyer, J.; Wang, E.; Hexemer, A.; Lee, S. W. Biomimetic Self-Templating Supramolecular Structures. *Nature* **2011**, *478*, 364–368.
3. Sun, B.; Sirringhaus, H. Surface Tension and Fluid Flow Driven Self-Assembly of Ordered ZnO Nanorod Films for High-Performance Field Effect Transistors. *J. Am. Chem. Soc.* **2006**, *128*, 16231–16237.
4. Duan, X.; Niu, C.; Sahi, V.; Chen, J.; Parce, J. W.; Empedocles, S.; Goldman, J. L. High-Performance Thin-Film Transistors Using Semiconductor Nanowires and Nanoribbons. *Nature* **2003**, *425*, 274–278.
5. Murphy, C. J.; Sau, T. K.; Gole, A. M.; Orendorff, C. J.; Gao, J.; Gou, L.; Hunyadi, S. E.; Li, T. Anisotropic Metal Nanoparticles: Synthesis, Assembly, and Optical Applications. *J. Phys. Chem. B* **2005**, *109*, 13857–13870.
6. Xia, Y.; Yang, P.; Sun, Y.; Wu, Y.; Mayers, B.; Gates, B.; Yin, Y.; Kim, F.; Yan, Y. One-Dimensional Nanostructures: Synthesis, Characterization, and Applications. *Adv. Mater.* **2003**, *15*, 353–389.
7. Hone, J.; Llaguno, M. C.; Nemes, N. M.; Johnson, A. T.; Fischer, J. E.; Walters, D. A.; Casavant, M. J.; Schmidt, J.; Smalley, R. E. Electrical and Thermal Transport Properties of Magnetically Aligned Single Wall Carbon Nanotube Films. *Appl. Phys. Lett.* **2000**, *77*, 666–668.
8. Wang, X.; Liu, Y.; Yu, G.; Xu, C.; Zhang, J.; Zhu, D. Anisotropic Electrical Transport Properties of Aligned Carbon Nanotube Films. *J. Phys. Chem. B* **2001**, *105*, 9422–9425.
9. Heo, K.; Cho, E.; Yang, J.-E.; Kim, M.-H.; Lee, M.; Lee, B. Y.; Kwon, S. G.; Lee, M.-S.; Jo, M.-H.; Choi, H.-J.; *et al.* Large-Scale Assembly of Silicon Nanowire Network-Based Devices Using Conventional Microfabrication Facilities. *Nano Lett.* **2008**, *8*, 4523–4527.
10. Rao, S. G.; Huang, L.; Setyawan, W.; Hong, S. Nanotube Electronics: Large-Scale Assembly of Carbon Nanotubes. *Nature* **2003**, *425*, 36–37.
11. Li, L.-S.; Alivisatos, A. P. Semiconductor Nanorod Liquid Crystals and Their Assembly on a Substrate. *Adv. Mater.* **2003**, *15*, 408–411.
12. Javey, A.; Nam; Friedman, R. S.; Yan, H.; Lieber, C. M. Layer-by-Layer Assembly of Nanowires for Three-Dimensional, Multifunctional Electronics. *Nano Lett.* **2007**, *7*, 773–777.
13. Fan, Z.; Ho, J. C.; Jacobson, Z. A.; Yerushalmi, R.; Alley, R. L.; Razavi, H.; Javey, A. Wafer-Scale Assembly of Highly Ordered Semiconductor Nanowire Arrays by Contact Printing. *Nano Lett.* **2007**, *8*, 20–25.
14. Takahashi, T.; Takei, K.; Ho, J. C.; Chueh, Y.-L.; Fan, Z.; Javey, A. Monolayer Resist for Patterned Contact Printing of Aligned Nanowire Arrays. *J. Am. Chem. Soc.* **2009**, *131*, 2102–2103.
15. Harnack, O.; Pacholski, C.; Weller, H.; Yasuda, A.; Wessels, J. M. Rectifying Behavior of Electrically Aligned ZnO Nanorods. *Nano Lett.* **2003**, *3*, 1097–1101.
16. Huang, Y.; Duan, X.; Wei, Q.; Lieber, C. M. Directed Assembly of One-Dimensional Nanostructures into Functional Networks. *Science* **2001**, *291*, 630–633.
17. Raez, J.; Moralez, J. G.; Fenniri, H. Long-Range Flow-Induced Alignment of Self-Assembled Rosette Nanotubes on Si/SiOx and Poly(methyl methacrylate)-Coated Si/SiOx. *J. Am. Chem. Soc.* **2004**, *126*, 16298–16299.
18. Kim, F.; Kwan, S.; Akana, J.; Yang, P. Langmuir-Blodgett Nanorod Assembly. *J. Am. Chem. Soc.* **2001**, *123*, 4360–4361.
19. Phillips, J. B.; Bunting, S. C. J.; Hall, S. M.; Brown, R. A. Neural Tissue Engineering: A Self-Organizing Collagen Guidance Conduit. *Tissue Eng.* **2005**, *11*, 1611–1617.
20. Crabb, R. A. B.; Chau, E. P.; Evans, M. C.; Barocas, V. H.; Hubel, A. Biomechanical and Microstructural Characteristics of a Collagen Film-Based Corneal Stroma Equivalent. *Tissue Eng.* **2006**, *12*, 1565–1575.
21. Zhu, Y.; Cao, Y.; Pan, J.; Liu, Y. Macro-Alignment of Electrospun Fibers For Vascular Tissue Engineering. *J. Biomed. Mater. Res., Part B* **2010**, *92B*, 508–516.
22. Wigmore, P. M.; Dunglison, G. F. The Generation of Fiber Diversity During Myogenesis. *Int. J. Dev. Biol.* **1998**, *42*, 117–125.
23. Papadaki, M.; Bursac, N.; Langer, R.; Merok, J.; Vunjak-Novakovic, G.; Freed, L. E. Tissue Engineering of Functional Cardiac Muscle: Molecular, Structural, and Electrophysiological Studies. *Am. J. Physiol.: Heart Circ. Physiol.* **2001**, *280*, H168–H178.
24. Grefte, S.; Kuijpers-Jagtman, A. M.; Torensma, R.; Von den Hoff, J. W. Skeletal Muscle Development and Regeneration. *Stem Cells Dev.* **2007**, *16*, 857–868.
25. Daley, W. P.; Peters, S. B.; Larsen, M. Extracellular Matrix Dynamics in Development and Regenerative Medicine. *J. Cell Sci.* **2008**, *121*, 255–264.
26. Lanfer, B.; Seib, F. P.; Freudenberg, U.; Stamov, D.; Bley, T.; Bornhauser, M.; Werner, C. The Growth and Differentiation of Mesenchymal Stem and Progenitor Cells Cultured on Aligned Collagen Matrices. *Biomaterials* **2009**, *30*, 5950–5958.
27. Rong, J.; Lee, L. A.; Li, K.; Harp, B.; Mello, C. M.; Niu, Z.; Wang, Q. Oriented Cell Growth on Self-Assembled Bacteriophage M13 Thin Films. *Chem. Commun.* **2008**, 5185–5187.
28. Wu, L.; Lee, L. A.; Niu, Z.; Ghoshroy, S.; Wang, Q. Visualizing Cell Extracellular Matrix (ECM) Deposited by Cells Cultured on Aligned Bacteriophage M13 Thin Films. *Langmuir* **2011**, *27*, 9490–9496.
29. Lin, Y.; Balizan, E.; Lee, L. A.; Niu, Z.; Wang, Q. Self-Assembly of Rodlike Bio-nanoparticles in Capillary Tubes. *Angew. Chem., Int. Ed.* **2010**, *49*, 868–872.
30. Lee, L. A.; Muhammad, S. M.; Nguyen, Q.; Sitasuwan, P.; Horvath, G.; Wang, Q. Multivalent Ligands Displayed on Plant Virus Induce Rapid Onset of Bone Differentiation. *Mol. Pharmaceutics* **2012**, *9*, 2121–2125.

31. Bruckman, M.; Kaur, G.; Lee, L. A.; Xie, F.; Sepulveda, J.; Breitenkamp, R.; Zhang, X.; Joralemon, M.; Russell, T. P.; Emrick, T.; *et al.* Surface Modification of Tobacco Mosaic Virus with Click Chemistry. *ChemBioChem* **2008**, *9*, 519–523.
32. Schlick, T. L.; Ding, Z.; Kovacs, E. W.; Francis, M. B. Dual-surface Modification of the Tobacco Mosaic Virus. *J. Am. Chem. Soc.* **2005**, *127*, 3718–3723.
33. Miller, R. A.; Presley, A. D.; Francis, M. B. Self-Assembling Light-Harvesting Systems from Synthetically Modified Tobacco Mosaic Virus Coat Proteins. *J. Am. Chem. Soc.* **2007**, *129*, 3104–3109.
34. Wu, L.; Zang, J.; Lee, L. A.; Niu, Z.; Horvatha, G. C.; Braxtona, V.; Wibowo, A. C.; Bruckman, M. A.; Ghoshroy, S.; zur Loye, H.-C.; *et al.* Electrospinning Fabrication, Structural and Mechanical Characterization of Rod-like Virus-Based Composite Nanofibers. *J. Mater. Chem.* **2011**, *21*, 8550–8557.
35. Kobayashi, M.; Seki, M.; Tabata, H.; Watanabe, Y.; Yamashita, I. Fabrication of Aligned Magnetic Nanoparticles Using Tobamoviruses. *Nano Lett.* **2010**, *10*, 773–776.
36. Kaur, G.; Valarmathi, M. T.; Potts, J. D.; Jabbari, E.; Sabo-Attwood, T.; Wang, Q. Regulation of Osteogenic Differentiation of Rat Bone Marrow Stromal Cells on 2D Nanorod Substrates. *Biomaterials* **2010**, *31*, 1732–1741.
37. Bruckman, M. A.; Hern, S.; Jiang, K.; Flask, C. A.; Yu, X.; Steinmetz, N. F. Tobacco Mosaic Virus Rods and Spheres as Supramolecular High-Relaxivity MRI Contrast Agents. *J. Mater. Chem. B* **2013**, *1*, 1482–1490.
38. Lee, L. A.; Nguyen, Q. L.; Wu, L.; Horyath, G.; Nelson, R. S.; Wang, Q. Mutant Plant Viruses with Cell Binding Motifs Provide Differential Adhesion Strengths and Morphologies. *Biomacromolecules* **2012**, *13*, 422–431.
39. Luckanagul, J.; Lee, L. A.; Shazly, T.; Nguyen, Q. L; Sitasuwan, P.; Yang, X.; Wang, Q. Porous Alginate Hydrogel Functionalized with Virus as Three-Dimensional Scaffolds for Bone Differentiation. *Biomacromolecules* **2012**, *13*, 3949–3958.
40. Sitasuwan, P.; Andrew Lee, L.; Bo, P.; Davis, E. N.; Lin, Y.; Wang, Q. A Plant Virus Substrate Induces Early Upregulation of BMP2 for Rapid Bone Formation. *Integr. Biol.* **2012**, *4*, 651–660.
41. Niu, Z.; Bruckman, M. A.; Li, S.; Lee, L. A.; Lee, B.; Pingali, S. V.; Thiyagarajan, P.; Wang, Q. Assembly of Tobacco Mosaic Virus into Fibrous and Macroscopic Bundled Arrays Mediated by Surface Aniline Polymerization. *Langmuir* **2007**, *23*, 6719–6724.
42. Lanfer, B.; Freudenberg, U.; Zimmermann, R.; Stamov, D.; Körber, V.; Werner, C. Aligned Fibrillar Collagen Matrices Obtained by Shear Flow Deposition. *Biomaterials* **2008**, *29*, 3888–3895.
43. Steinmetz, N. F.; Mertens, M. E.; Taurog, R. E.; Johnson, J. E.; Commandeur, U.; Fischer, R.; Manchester, M. Potato Virus X as a Novel Platform for Potential Biomedical Applications. *Nano Lett.* **2009**, *10*, 305–312.
44. Niu, Z.; Liu, J.; Lee, L. A.; Bruckman, M.; Zhao, D.; Koley, G.; Wang, Q. Biological Templated Synthesis of Water-Soluble Conductive Polymeric Nanowires. *Nano Lett.* **2007**, *7*, 3729–3733.
45. Niu, Z.; Bruckman, M.; Harp, B.; Mello, C.; Wang, Q. Bacteriophage M13 as a Scaffold for Preparing Conductive Polymeric Composite Fibers. *Nano Res.* **2008**, *1*, 235–241.
46. Dogic, Z.; Fraden, S. Smectic Phase in a Colloidal Suspension of Semiflexible Virus Particles. *Phys. Rev. Lett.* **1997**, *78*, 2417–2420.
47. Khalil, A. S.; Ferrer, J. M.; Brau, R. R.; Kottmann, S. T.; Noren, C. J.; Lang, M. J.; Belcher, A. M. Single M13 Bacteriophage Tethering and Stretching. *Proc. Natl. Acad. Sci. U. S. A.* **2007**, *104*, 4892–4897.
48. Li, T.; Zan, X.; Winans, R. E.; Wang, Q.; Lee, B. Biomolecular Assembly of Thermoresponsive Superlattices of the Tobacco Mosaic Virus with Large Tunable Interparticle Distances. *Angew. Chem., Int. Ed.* **2013**, *52*, 6638–6642.
49. Wang, X.; Niu, Z.; Li, S.; Wang, Q.; Li, X. Nanomechanical Characterization of Polyaniline Coated Tobacco Mosaic Virus Nanotubes. *J. Biomed. Mater., Res. Part A* **2008**, *87A*, 8–14.
50. Petrova, H.; Perez-Juste, J.; Zhang, Z.; Zhang, J.; Kosel, T.; Hartland, G. V. Crystal Structure Dependence of the Elastic Constants of Gold Nanorods. *J. Mater. Chem.* **2006**, *16*, 3957–3963.
51. Menagen, G.; Macdonald, J. E.; Shemesh, Y.; Popov, I.; Banin, U. Au Growth on Semiconductor Nanorods: Photo-induced *versus* Thermal Growth Mechanisms. *J. Am. Chem. Soc.* **2009**, *131*, 17406–17411.
52. Chaney, S. B.; Shanmukh, S.; Dluhy, R. A.; Zhao, Y. Aligned Silver Nanorod Arrays Produce High Sensitivity Surface-Enhanced Raman Spectroscopy Substrates. *Appl. Phys. Lett.* **2005**, *87*, 0319081–0319083.
53. Perez-Juste, J.; Rodriguez-Gonzalez, B.; Mulvaney, P.; Liz-Marzan, L. M. Optical Control and Patterning of Gold-nanorod-poly(vinyl alcohol) Nanocomposite Films. *Adv. Funct. Mater.* **2005**, *15*, 1065–1071.
54. Aubin, H.; Nichol, J. W.; Hutson, C. B.; Bae, H.; Sieminski, A. L.; Cropek, D. M.; Akhyari, P.; Khademhosseini, A. Directed 3D Cell Alignment and Elongation in Microengineered Hydrogels. *Biomaterials* **2010**, *31*, 6941–6951.
55. Faureau, C.; Delbarre, E.; Courvalin, J. C.; Buendia, B. Differentiation of C2C12 Myoblasts Expressing Lamin A Mutated at a Site Responsible for Emery-Dreifuss Muscular Dystrophy is Improved by Inhibition of the MEK-ERK Pathway and Stimulation of the PI3-kinase Pathway. *Exp. Cell. Res.* **2008**, *314*, 1392–1405.
56. Li, B.; Lin, M.; Tang, Y.; Wang, B.; Wang, J. H. C. A Novel Functional Assessment of the Differentiation of Micropatterned Muscle Cells. *J. Biomech.* **2008**, *41*, 3349–3353.
57. Fanzani, A.; Stoppani, E.; Gualandi, L.; Giuliani, R.; Galbiati, F.; Rossi, S.; Fra, A.; Preti, A.; Marchesini, S. Phenotypic Behavior of C2C12 Myoblasts upon Expression of the Dystrophy-Related Caveolin-3 P104L and TFT Mutants. *FEBS Lett.* **2007**, *581*, 5099–5104.
58. Bajaj, P.; Reddy, B.; Millet, L.; Wei, C. N.; Zorlutuna, P.; Bao, G.; Bashir, R. Patterning the Differentiation of C2C12 Skeletal Myoblasts. *Integr. Biol.* **2011**, *3*, 897–909.
59. Kaur, G.; Wang, C.; Sun, J.; Wang, Q. The Synergistic Effects of Multivalent Ligand Display and Nanotopography on Osteogenic Differentiation of Rat Bone Marrow Stem Cells. *Biomaterials* **2010**, *31*, 5813–5824.
60. Zan, X.; Sitasuwan, P.; Powell, J.; Dreher, T. W.; Wang, Q. Polyvalent Display of RGD Motifs on Turnip Yellow Mosaic Virus for Enhanced Stem Cell Adhesion and Spreading. *Acta Biomater.* **2012**, *8*, 2978–2985.
61. Sun, Y.; Ge, Y.; Dmevich, J.; Zhao, Y.; Band, M.; Chen, J. Mammalian Target of Rapamycin Regulates mi-RNA-1 and Follistatin in Skeletal Myogenesis. *J. Cell. Biol.* **2010**, *189*, 1157–1169.
62. Boontheekul, T.; Kong, H.-J.; Hsiong, S. X.; Huang, Y.-C.; Mahadevan, L.; Vandenburgh, H.; Mooney, D. J. Quantifying the Relation Between Bond Number and Myoblast Proliferation. *Faraday Discuss.* **2008**, *139*, 53–70.
63. Rowley, J. A.; Mooney, D. J. Alginate Type and RGD Density Control Myoblast Phenotype. *J. Biomed. Mater. Res.* **2002**, *60*, 217–223.
64. Wang, P.-Y.; Thissen, H.; Tsai, W.-B. The Roles of RGD and Grooved Topography in the Adhesion, Morphology, and Differentiation of C2C12 Skeletal Myoblasts. *Biotechnol. Bioeng.* **2012**, *109*, 2104–2115.
65. Wang, P.-Y.; Yu, H.-T.; Tsai, W.-B. Modulation of Alignment and Differentiation of Skeletal Myoblasts by Submicron Ridges/Grooves Surface Structure. *Biotechnol. Bioeng.* **2010**, *106*, 285–294.
66. Olson, E. N. Interplay between Proliferation and Differentiation within the Myogenic Lineage. *Dev. Biol.* **1992**, *154*, 261–272.
67. Clark, P.; Dunn, G. A.; Knibbs, A.; Peckham, M. Alignment of Myoblasts on Ultrafine Gratings Inhibits Fusion *in Vitro*. *Int. J. Biochem. Cell Biol.* **2002**, *34*, 816–825.
68. Li, K.; Chen, Y.; Li, S.; Nguyen, H. G.; Niu, Z.; You, S.; Mello, C. M.; Lu, X.; Wang, Q. Chemical Modification of M13

Bacteriophage and Its Application in Cancer Cell Imaging. *Bioconjugate Chem.* **2010**, *21*, 1369–1377.
69. Niu, Z.; Bruckman, M.; Kotakadi, V. S.; He, J.; Emrick, T.; Russell, T. P.; Yang, L.; Wang, Q. Study and Characterization of Tobacco Mosaic Virus Head-to-Tail Assembly Assisted by Aniline Polymerization. *Chem. Commun.* **2006**, 3019–3021.